ACCELERATOR FACILITIES IN THE 100-1000 TEV RANGE

W.A. Wenzel
Lawrence Berkeley Laboratory
Berkeley, California

Summary

The application of current technologies to proton-antiproton colliders of 20, 100 and 1000 TeV is studied. The maximum field in the superconducting magnets is 2 or 5 Tesla. The facility also includes a conventional ring for electrons and positrons with two to three orders of magnitude less energy. An unique injector employs a rapid cycling, variable tune superconducting ring to accelerate particles from 10 GeV to the minimum operating momentum of the storage accelerator.

The scaling of costs with momentum is minimized in several ways. Extensive beam-beam feedback for orbit control permits the use of small apertures. The very long magnets are produced on a linear assembly line. Finally, the accelerators are combined into a three ring circus maximus within a single neutral buoyance cryostat supported in a water-pipe tunnel of small diameter.

The creation with current technologies of 100-1000 TeV accelerators may not be completely inconceivable; but some significant departures from current design philosophies are needed. For example,

1. The fabrication of very long, small aperture superconducting magnets requires a linear assembly line approach.
2. "Smart" detectors and processors must use beam position information for on line orbit correction and to damp instabilities.
3. A modest but selective site development is required. In particular elaborate tunnels must be avoided.

In addition some priority among scientific goals is needed so that design compromises can be compared realistically. High energy, high luminosity, good duty cycle and efficient beam extraction, for example, create additive (if not multiplicative) problems affecting both feasibility and cost.

In what follows we suggest an approach to P-$\bar{P}$ colliders which is intended to explore the implications of a single very large step beyond current facilities. Some of these may be useful for a machine in the 20 TeV range[1], for which parameters are also included.

I. General Plan

The proton and antiproton sources use Tevatron-like 10 GeV rings for accumulation, cooling and preliminary acceleration. Figure 1 shows the storage accelerator ring carried in a single cryostat with a superconducting injection ring of lower field and a conventional magnet ring to help with injection and for $e^{\pm}$ storage. At intersection regions the rings are separated radially using straight sections which occupy a very small part of the circumference.

Short straight sections between long magnets alternate in function between cryogenic and warm services (Figure 2). At several dozen stations beam position and phase information, received just ahead of beam arrival, is used for fast orbit corrections. Relatively slow site movement and atmospheric changes are monitored using microwave interferometry across radii and sectors, optical registration of beam line elements within the cryostat and measured beam position.

Site development is minimal. There are several experimental intersection regions, a dedicated gigawatt power station, a ring-oriented network of ac, dc and radio frequency power, communication and computing equipment, refrigerators and correction magnets. The magnet ring follows smooth elevation changes in the surface. The neutral-buoyancy cryostat is suspended in water inside a pipe buried at modest depth (Figure 1). Relatively large ($\geq$ 10mm) transverse displacements of the cryostat can be carried out within minutes.

For the storage accelerator two values of the magnetic field, 2 T and 5 T, and three energies, 20 100 and 1000 TeV are considered. Because the availability of suitable sites on land is obviously limited, especially at 1000 TeV, the examination of alternative designs for the ocean or outer space is an appropriate exercise for the reader.

II. Magnet and Ring Design and Construction

A. General Features

In several respects the superconducting magnet design departs from conventional approaches.

1. All normal lattice magnets are idential. The number is minimized by making them long.
2. Full length separately powered (Figure 3) current elements of simple shapes give complete flexibility in the azimuthal current distribution. The required multipole distribution of the magnetic field, therefore, is readily achieved at all levels of excitation.
3. The use of wedge-shaped conductors in the high field storage accelerator (Figure 4) permits necessary stress loading from the outside radius.
4. The magnet-core assembly line is linear; the fabrication technique is independent of magnet length.
5. The cryostat for the small aperture magnet uses a very light-weight support system to minimize heat losses.
6. An unique injector is proposed for consideration. This uses spiral quadrupole windings (Figure 4) to obtain short betatron wavelengths at low momenta.

B. Superconducting Coil

1. Superconductor

We assume that the superconductor is a commonly used monolithic intrinsically stable Cu-NbTi matrix with 10 μm diameter NbTi filaments and a twist pitch of 0.01m. For a Cu/SC ratio of 1.8 the critical currents are 0.6×10^9 A/m^2 at 5T and 1.2×10^9 A/m^2 at 2T.[2] The conductor shapes vary from 13mm-deep wedges at 5T to millimeter strips at 2T and even thinner layers for the injector. Table I gives approximate superconductor requirements for the storage accelerator.

For simplicity we have assumed that all magnet apertures are the same. Because of the strong dependence on radius of some transverse beam instabilities, it is likely that at 2T the aperture would have to be larger than at 5T. This offsets to some extent the advantages of low fields in the overall magnet hardware requirements.

At 5T some savings in the amount of superconductor could be made with a double layer (dotted line in Figure 4) of wedges operated with different current densities or superconductor ratios. For fields above 5T this alternative would probably be necessary.

2. Magnet Current

Figure 3 shows schematically how the magnets are powered. A central facility distributes as a function of time digital signals specifying the magnet currents in all windings. The required number of combinations of dipole, quadrupole and sextupole components is small. Local corrections can be added for non-planarity of orbit and those misalignments which cannot be removed by adjusting the cryostat position.

3. Stored Energy and Quench Protection

The stored energy inside the inner coil radius a is given by

$$\text{Energy (J/m)} = 10^7\ a^2\ B^2/8 \qquad (1)$$

In the absence of any magnetic shielding, the total stored energy is larger by a factor, $1+2b/3a+b^2/3a^2$ where b is the coil outer radius. For the 5T field, where the steel helps only a little, the stored energy exceeds 10 MJ/km. At 2T it is approximately 1 MJ/km.

For internal quench protection the coil configuration proposed here has some advantages over the familiar pancake design, because current elements occupying only small azimuthal intervals are separately powered. In the event of a quench the increase in terminal voltage effectively disconnects the power source of the quenching element, shifting current to the neighboring elements and leaving the stored energy distribution essentially unchanged. Because each power supply is current regulated, these additional currents are supplied through the terminal resistors. Whether or not the neighboring elements quench immediately, all the terminal resistors share in the dissipation of the stored energy. The beam tube also will carry axial current. Its heating will both absorb energy and help spread the quench.

C. Magnet Core

In operation the magnet steel and the beam tube are cold. The full length insulated conductors are assembled radially against a thin beam tube, then squeezed by a laminated steel core which provides necessary hoop stress, confines the magnetic flux and permits axial displacement to accommodate the differential thermal contraction of one part in 1000 between superconductor and steel. Because the magnet has relatively little axial stiffness, the assembly line terminates with a large drum on which the core is wound like a cable.

In a relatively conventional approach pairs of stamped laminates could be stacked around the coil. The cooling tubes could serve as stacking guides and then squeezed to apply radial force. Because of the relatively small coil diameter, the hoop stresses even at 5T are relatively small. It might be sufficient to glue (rather than weld) the structure together.

Figure 4 shows an alternative approach which might be well suited to long assembly lines. The conductor is wrapped with steel wire or narrow strips in helical layers of alternating helicity. It remains to be learned how well the azimuthal wrapping forces and the resultant twists can be cancelled. Small residual twists can be controlled using gravity and the positioning of the cryostat inside its waterbed. In spite of their great lengths the magnets are thin lenses, so that average values for coil position and axis alignment are most important.

For simplicity Figures 1 and 4 show circular apertures for the magnets. For the storage accelerator an elliptical cross section is probably appropriate and is consistent with the fabrication procedure. For the low field superconducting injector the circular aperture is necessary, so that two quadrupole ($\cos 2\phi$ current distribution) coils can be spirally wrapped to produce many short alternating gradient magnet elements within each long cryostat. Because circular symmetry is required for these quadrupole windings, careful keying is needed to preserve the orientation of the dipole windings.

D. "Tunnel" and Cryostat Support (Figure 1)

Each magnet cryostat is supported in a water filled pipe buried 2-3m deep, as required for radiation safety and to achieve a smooth, not necessarily planar, orbit. Deep cutting and tunnelling are needed only for locally steep terrain or to avoid population centers and other immovable objects.

Both water pipe and cryostat shell, including separate sets of rails for warm and cold inserts, are assembled in situ from short ($\lesssim$ 50m-long) sections. These are joined with very short ($\lesssim$ 0.1m-long) transition sections which hold the pulleys and cables which support the cryostat. The cables run inside the water pipe to the ends of each magnet section where they can be used to adjust the transverse positions of the magnets.

At each end of each magnet the cryostat and water pipe are joined with a bellows which provides several centimeters of relative transverse motion. The tolerances on this assembly are obviously very loose. Nevertheless, the magnet can be aligned precisely by optical sighting through the (cold part of the) cryostat.

E. Assembly into Cryostat

Each magnet core is inserted into its cryostat in situ using a mini-assembly line at the warm service straight section. As it is unwound from the storage drum the core of the storage accelerator, with cooling tubes and injector ring, is clamped at intervals of $\sim$1m and wrapped with superinsulation and an intermediate heat shield. Rollers which ride on two rails on the cryostat wall are each attached with two fiberglass strings to the cooling tubes near the clamps. Other rails on the cryostat inner wall are used to support the third (conventional) magnet ring and to carry warm services such as distributed vacuum pumps.

During magnet installation the empty cryostat rests on the bottom of the empty water pipe. Longitudinal forces of the order of a ton, necessary to overcome roller friction and/or gravity, are provided by pulling on the cooling tubes. The magnet elements will recede at cooldown from the warm service stations by 3 parts in 1000 of their lengths. During warmup, tension may be needed to keep the core from buckling.

With the magnet installed the support pipe is filled with water. The cryostat support interval can be made as large as 50m by carefully adjusting the cryostat density. Ballast tubes filled with air or water could be used. The density of water changes by only one part in 1000 for a 4°C change in temperature.

F. Cryogenics

Refrigeration may be the largest single expense. The proposed magnet support system is intended to minimize this, but it will be hard to get the losses to the wall of the cryostat below 100W per km. In the longest ring considered here (1000 TeV at 2T) this would require ~1MW of cold power. The efficiency of the refrigeration system must be examined carefully. Heat exchangers within the cryostat, for example, could be used to precool helium coming into the refrigerators.

Another source of heating is from the cycling of the superconductors, which produces a hysteresis loss given by[2]

$$G_o \ (J/m^3 \text{ cycle}) = i_c \, d_f \, \lambda \Delta B \qquad (2)$$

where i_c is the critical current, d_f is the filament diameter, ΔB is the field change and λ is the fraction of superconductor in the matrix. Taking $i_c \, \Delta B = 2.4 \times 10^9 \ ATm^{-2}$, $\lambda = 0.36$, $d_f = 10 \ \mu m$, we find $G_o = 8640 \ J/m^3$ cycle. The amount of superconductor in the (5T) storage accelerator is at most a cubic meter per km, so even for a relatively short 1000 sec ramping time, the hysteresis power is $<10W/km$, much smaller than the assumed total loss of 100 W/km. For the injector the fields are lower by more than an order of magnitude. Because the required area of superconductor goes inversely as the square of the field strength, the injector cycle time may be as low as a few seconds.

III. Orbits and Optics

A. General

The momentum P, dipole magnetic field B and radius R are related by P = 0.3 BR (Table I). We assume the circumference factor is unity, a good approximation in view of the design featuring relatively few combined function magnets separated by short straight sections.

1. Orbit corrections

Fast beam-beam feedback can be used to correct orbits, damp instabilities and perhaps to reduce emittance. The differential elapsed time Δt between (beam) arc and (signal) chord routes for angular width ψ is given by

$$\Delta t = R[\psi - 2 \sin(\psi/2)]/c \text{ or } \psi \approx (24c\Delta t/R)^{1/3} \qquad (3)$$

Table I shows the number $(2\pi/\psi)$ of independent feedback arcs per revolution. We have used $\Delta t = 100$ nsec to accommodate amplifier delays and signal routing to and from the transmitters and receivers.

2. Betatron tune and relative quadrupole strength

The magnet number N and length L, the tune Q and the phase shift u per alternating gradient cell of length 2L are related by

$$NL = 2\pi R, \ Nu = 4\pi Q, \text{ or } L = Ru/2Q \qquad (4)$$

u is also related to the focal length F per cell and the field gradient B′ by

$$u = (2L/F)^{\frac{1}{2}} = 2L^2B'/\sqrt{3}BR, \text{ hence} \qquad (5)$$

$$B_q/B = 2\sqrt{3} \, aQ^2/Ru \qquad (6)$$

where $B_q \equiv aB'$ is the quadrupole field at the inner coil radius a.

A similar relationship applies to separated function lattices provided that the ratio of field strengths is multiplied by the ratio of quadrupole to dipole magnet lengths. With this correspondence, the Fermilab Main Ring, with quadrupole aperture a = 0.05m, R = 1km, Q = 20, u = 1.25 gives $aQ^2/Ru = 0.016$ or $L_qB_q/LB = 0.055$. The Main Ring has approximately twice this ratio of magnet length devoted to quadrupoles because the circumference factor is appreciably less than unity and because the poletip fields are smaller for the quadrupoles than for the dipoles (1.2 T vs 1.8 T at 400 GeV).

3. Magnet sagitta

The sagitta S of each magnet is given by

$$S = L^2/8R = 2a/64 \ (aQ^2/Ru^2) \qquad (7)$$

For $aQ^2/Ru \gtrsim 0.016u$, therefore, it is possible, independent of design energy, to sight through the aperture of each magnet. Usually the phase shift per cell is limited to the range $\pi/3 \leq u \leq \pi/2$. In any case the cold part of the cryostat, as shown in Figure 1, provides plenty of width for optical alignment.

4. Dispersions of orbit radius and frequency

From the relationship between the momentum compaction factor α and Q, i.e.

$$\alpha \equiv (dR/R)/(dP/P) \approx Q^{-2} \qquad (8)$$

the radial displacement ΔR associated with momentum width ΔP is given by

$$\Delta R = R\Delta P/PQ^2 = a \ (\Delta P/P)/(aQ^2/R) \qquad (9)$$

The factor aQ^2/R, therefore, determines also the effect of fractional field errors on the relative (to aperture) orbit displacement.

The frequency dispersion η is related to α by

$$\eta \equiv (d\omega/\omega)/(dP/P) \equiv \gamma^{-2} - \alpha \approx \gamma^{-2} - Q^{-2} \qquad (10)$$

where $\omega \equiv v/r$. Phase transition occurs at $\gamma = Q$.

B. Storage Accelerator

Table I gives parameters for the storage accelerator. We take $u_s = 1$, $a_s = 13$mm, $a_sQ_s^2/R = 0.013$. In all cases the storage accelerator operates above transition energy. From equation 9 the closed orbit sensitivity is given by $\Delta R/a_s = 80 \ \Delta P/P$, indicating that field errors must be corrected to better than one percent of the injection field.

C. Injector

Injection into the storage accelerator could follow current practice of successive injection into and extraction from a series of relatively high field synchrotron rings. For the very large overall momentum ratio required here several such rings would be required. Although the sum of the circumferences of these rings would be much less than for the

storage accelerator, the relative cost of the injection system would not necessarily be small because comparable economies of scale would not apply. Furthermore the gymnastics of many beam transfers, although persumably straightforward, could be time consuming.

For injection we propose to consider an unusual alternative -- a full radius variable tune ring to carry particles from preinjection at P_o = 10 GeV to storage accelerator injection at P_2. To offset the effect of fixed field errors, a very large betatron tune is required at low momenta. Short lenses for this purpose use spiral windings with a cos 2ϕ current distribution (Figure 4). The superposition of opposite helicity windings gives a field gradient that varies sinusoidally along the orbit with an effective strength that is two-thirds the maximum. The alternating gradient cell length $2L_o$ is equal to half the winding pitch.

1. Quadrupole strength

Proceeding as in III.A. above we find that as a function of momentum-dependent injector parameters (subscript i)

$$L_o = Ru_o/2Q_o = Ru_i/2Q_i, \text{ and}$$
$$B_{qi}/B_i = 3\sqrt{3}\, a_o Q_i^2/Ru_i \qquad (11)$$

From equation 9 we infer that $P_i Q_i^2$ = const. is the appropriate scaling law for injector tune. This gives,

$$B_{qi}/B_i = 3\sqrt{3}\,(a_o Q_2^2/Ru_o)\, P_2/(P_o P_i)^{\frac{1}{2}}, \text{ and}$$
$$B_{q2}/B_2 = 3\sqrt{3}\,(a_o Q_2^2/Ru_o)(P_2/P_o)^{\frac{1}{2}} \qquad (12)$$

Table I shows injector parameters for a_o = 13mm, u_o = 1, P_2 = 0.05 P_s and $Q_2 = Q_s$. Note that for $u_2 = u_s$, $L/L_o = (P_2/P_o)^{\frac{1}{2}}$.

2. Two stage injector

At the highest energies considered here, $B_{q2} > B_2$. The total field, $B_{q2} + B_2$, is still small enough to avoid saturation of the magnet steel, an effect that would seriously jeopardize the field quality. Nevertheless the total amount of steel and superconductor can be reduced if an additional set of quadrupole windings is added. These would give a stronger lens of length L_1, for use when $P_1 \le P_i \le P_2$. The initial lens of length L_o would be used for $P_o \le P_i \le P_1$. The quadrupole field is minimized by choosing $P_1 = (P_o P_2)^{\frac{1}{2}}$, and $u_1 = u_o$. This gives $L_1/L_o = (P_2/P_o)^{\frac{1}{4}}$. In this case the quadrupole field at P_1 obtained with lens length L_o and at P_2 with length L_1 are equal and are given by

$$B_{q2}/B_2 = 3\sqrt{3}\,(a_o Q_2^2/Ru_o)(P_2/P_o)^{\frac{1}{4}} \qquad (13)$$

smaller by a factor $(P_2/P_o)^{\frac{1}{4}}$ than for the one lens injector design. For this choice of P_1 the two stage injector parameters are also given in Table I. Alternatively, and with little difference, P_1 could be chosen equal to the electron momentum for the conventional third ring discussed below.

3. Betatron damping and phase transition

For the variable Q injector the transverse amplitude y is damped[3] according to

$$\langle y \rangle \propto (PQ)^{-\frac{1}{2}} \propto P^{-\frac{1}{4}} \qquad (14)$$

to be compared with a $P^{-\frac{1}{2}}$ dependence for fixed Q accelerators. The transverse slope is damped according to $\langle y' \rangle \propto Q \langle y \rangle$. The transverse emittance, therefore, goes as

$$\langle y \rangle \langle y' \rangle \propto QP^{-\frac{1}{2}} \propto 1/P \qquad (15)$$

the same as for fixed Q accelerators.

From equation 10, phase transition for the injector occurs at

$$P_t = M Q_t = (M^2 P_2 Q_2^2)^{1/3} \qquad (16)$$

For all cases considered here (Table I), $P_1 < P_t < P_2$.

4. Orbit stability

During acceleration the tune may have to be jumped over harmonics associated with magnet and cell lengths L and 2L. These occur for

$$Q_i = 4\pi Q_s/u_s \text{ and } 2\pi Q_s/u_s \qquad (17)$$

or, given $Q_2 = Q_s$ and $u_s = 1$, at $P_i/P_2 = 0.0063$ and 0.025, respectively.

Generally the orbit characteristics of the variable Q injector differ in very important ways from those of the conventional fixed tune machine. For the latter the betatron amplitude produced by a periodic perturbation is bounded, through phase closure, by a value inversely proportional, for example, to the phase difference from the nearest harmonic resonance. In the variable Q injector on the other hand, steady state operation is impossible at low energies, where Q is so large that the chromatic effects cannot be sufficiently corrected to avoid such resonances and stop bands.

During acceleration these effects don't matter directly, because Q changes so rapidly that for each particle the betatron phase at any point on the ring is effectively random from cycle to cycle. A local perturbation, therefore, creates a series of random changes in betatron amplitude. Although average effects are readily corrected by using beam-beam feedback, the random nature of individual particle histories can lead to some stochastic increase in emittance. Note that for the fixed tune accelerators a similar problem exists if there are random perturbations from, say, ground motion with frequencies near or larger than the orbital frequency, a range of more than two orders of magnitude for the facilities considered here.

At $P_i = P_2$, where we set $Q_2 = Q_s$, the injector could presumably operate as a storage accelerator, although it will be desirable to avoid paying too much for field quality.

IV. Injector Operation

For the intense antiproton source the injector would be cycled very rapidly (> 1 Hz) to provide protons of a few hundred GeV, optimum for producing antiprotrons in the 10 GeV range. Similarly, the rapid acceleration of small electron bunches to fill the conventional ring for $e^{\pm}$ collider operation will avoid overloading the cryogenic system with synchrotron radiation. The latter goal will also be achieved by injecting somewhat below $e^{\pm}$ operating energy. For these applications only the short lens system is needed.

The two stage injector is especially well suited to preliminary stacking before injection into the storage accelerator. Fed by the injector at momentum P_1, the third (conventional) ring would accumulate and stack small bunches of protons or antiprotons. The larger (stacked) bunches would then be accelerated from P_1 to P_2 using the second lens system. This process would not only avoid changing between injector lens systems during a single acceleration, but it would save r.f. power by reducing the number of "trips" to P_2. Also, by involving the conventional ring, this procedure would minimize losses in particle transfers to the cryogenic system.

In summary, the variable Q injector is used at low energies like a low gradient (~three orders of magnitude lower than SLAC's) linac. Relative to linear linacs its advantages are that the hardware is recycled and that the ring can be made "smart" because of the curvature. Relative to fixed tune injection synchrotrons its advantages include an enourmous momentum range in one ring, plus the fact that it is matched to otherwise necessary characteristics of the "tunnel" and cryostat.

V. Conventional Third Ring

The electron-positron collider ring is made of conventional materials because of both the intense synchrotron radiation and the very low dipole field strength. Its alternative use in proton-antiproton injection is described above.

For picture-frame dipoles the power and conductor volume are related to the momentum P (GeV), gap g (m) and resistivity ρ (ohm-m) by

$$\text{Power x Volume } (\text{MWm}^3) = 10^{10}\,\rho P^2 g^2/9 \qquad (18)$$

For $\cos\phi$ dipoles with thin coils, multiply by $\pi^2/8$. Independent of ring circumference, therefore, the metal in the Fermilab Main Ring could in principle be reshaped to provide a 1 TeV third ring at the same power level presently required at 500 GeV for twice our third ring vertical aperture. For $R\sim10^6$m, the coil thickness would be only ~1mm. The steel would be very thin and the cycle rate could, if necessary, be large.

Because the operating dipole field B_e is very low for the facilities studied here, a careful magnet design using several layers of magnetic shielding is needed. Also the betatron tune should be as large as possible. If both magnet power and conductor volume are doubled, the quadrupole and dipole fields can be made equal. Assuming for simplicity of comparison that a conductor configuration like that of the injector is used, the tune is determined by

$$B_{qe}/B_e = 1 = 3\sqrt{3}\,a_e Q_e^2/Ru_e \qquad (19)$$

Taking a_e = 13mm and u_e = 1, we find $Q_e = 3.8Q_s$.

VI. Synchrotron Radiation

For B in Tesla and both M and E in GeV, the energy loss per turn per particle is

$$U = 4\pi r_p M_p \gamma^4/3R = 1.81\cdot10^{-18}\ BE^3/M^4 \ \text{(GeV)} \qquad (20)$$

where $r_p = 1.53\cdot10^{-18}$ m and M_p = 0.938 GeV

The damping time T is given by

$$T = 2E/(dE/dt) = 0.77\cdot10^{11}\ M^4/B^2\,E \ \text{(sec)} \qquad (21)$$

The radiated power per particle is

$$\text{Power} = 4.15\cdot10^{-21}\ B^2E^2/M^4 \ \text{(W)} \qquad (22)$$

The radiated power gradient per particle is

$$d\ (\text{Power})/ds = 1.98\cdot10^{-22}\ B^3E/M^4 \ \text{(W/m)} \qquad (23)$$

The critical energy is

$$E_c = 3\hbar c\gamma^3/2R = 0.89\cdot10^{-10}\ BE^2/M^3 \ \text{(keV)} \qquad (24)$$

Table II shows that synchrotron radiation can provide useful damping for P-$\bar{P}$. If the number of stored protons is large, refrigeration losses in the cryostat can be a problem. A possible solution is to make the aperture wider radially in order to insert warm absorbers at regular intervals. The critical energies are low enough for absorption of the synchrotron energy in short lengths of heavy metal.

In the Table we show the radiation loss for $N_p = 10^{15}$. At the higher energies the power gradient for radiation loss greatly exceeds the total assumed for the support structure (100W/km). This implies either a smaller circulating beam or a design in which the synchrotron radiation can be collected on warm surfaces.

For the electrons the radiation determines both the operating energy E_e and the number N_e or current I_e. For the collider to function as a synchrotron we assume that the energy loss per turn is a modest fraction of the total energy. Arbitrarily we set

$$U_e/E_e \equiv f_e = 0.05 \qquad (25)$$

This determines the energy and gives a critical energy that is independent of B and E, i.e.

$$E_c = 9f_e\ (mc^2)/8\pi(e^2/\hbar c) = 1.25\ \text{MeV} \qquad (26)$$

It is apparent that refrigeration for the protons and r.f. power for the electrons, together with the stored beam energy, place strong limits on the numbers of circulating particles and, therefore, on the achievable luminosities.

VII. Conclusions

From the wide range of momenta and field strengths considered here some, certainly not all, of the problems of applying present technologies to much larger facilities are perceived. It is at best sobering, and at worst impossible, to conceive the construction of a 1000 TeV facility in, say, five shift-years (10^4 hours), during which the assembly line(s) will have to produce and install almost everything at a rate of 1 km per hour.

A particularly significant cost factor for very high energy superconducting facilities is refrigeration. If synchrotron radiation must be absorbed in the magnet the circulating beam will be limited significantly in intensity. The alternative of absorbing the synchrotron radiation on warm surfaces requires a more elaborate magnet structure and support system and implies a much larger ambient heat load. Improvements in refrigeration efficiencies can help. This is an application where the development of a higher temperature superconductor would be especially welcome.

Independent of refrigeration problems, the stored energies in the proton beams are terrifying, primarily because the magnet can be destroyed unless

beam extraction, emergency and otherwise, is 100 percent efficient. It is essential, therefore, that experimenters and theorists continue to examine beam requirements. A given number of particles will provide higher collider luminosity if the number of bunches is small. But the duty cycle will then be worse for both collider and fixed target experiments. This trade-off alone justifies considerable effort on both detector development and simulation studies to help extract significant results from junk-dominated hadron interactions.

One advantage of studying the implications of very large extrapolations is that better approaches to relatively modest steps may also be encouraged. At 20 TeV, for example, most of the problems considered here are relatively small. Departure from current practices for technical reasons seems unnecessary, but the effort, time and cost of building even this small facility may dicate otherwise.

References

1. ICFA Workshops; FNAL, April 1979; Les Diablerets, October, 1979.
2. M.A. Green, Ph.D. thesis; May, 1977, LBL-5350.
3. Henri Bruck, Accelerateurs Circulaires de Particles. Presses Universitaries de France.

TABLE I - Magnet Ring Parameters. P_o = 10 GeV, $Q_2 = Q_s$, $a_s = a_o = a_e$ = 13 mm, $u_s = u_o = u_1 = u_e = 1$.

Storage Accelerator						
P_s (TeV)	20		100		1000	
B_s (T)	2	5	2	5	2	5
R (km)	33.3	13.3	167	67	1670	670
$2\pi/\psi$ (feedback)	23	17	39	28	83	61
B_{qs} (T)	0.090	0.225	0.090	0.225	0.090	0.225
Q_s (tune)	183	116	408	258	1290	816
L (m)	91	58	204	129	645	408
N (magnet no.)	2300	1450	5130	3240	16200	10300
S/C coil: Vol (m^3)	17	89	86	445	860	4450
(b-a) (mm)	1.3	13	1.3	13	1.3	13
Injector						
P_2 (TeV)	1	1	5	5	50	50
P_f (TeV)	0.31	0.23	0.90	0.66	4.2	3.1
B_2 (G)	1000	2500	1000	2500	1000	2500
B_{q2} (G)	675	1690	1510	3780	4780	11940
B_o (G)	10	25	2	5	0.2	0.5
B_{qo} (G)	67.5	169	67.5	169	67.5	169
Q_o	1830	1160	9130	5770	91300	57700
L_o (m)	9.1	5.8	9.1	5.8	9.1	5.8
Inj. (2nd stage)						
P_1 (TeV)	0.100	0.100	0.224	0.224	0.707	0.707
B_1 (G)	100	250	45	112	14	35
B_{q2} (G)	210	530	320	800	570	1420
Q_1	577	365	1930	1220	10900	6860
L_1 (m)	29	18	43	27	77	49
Electron Ring						
P_e (TeV)	0.266	0.196	0.456	0.336	0.980	0.722
$B_e = B_{qe}$ (G)	266	490	91	168	20	36
Q_e	700	440	1570	990	4970	3140
L_e (m)	24	15	53	34	168	106

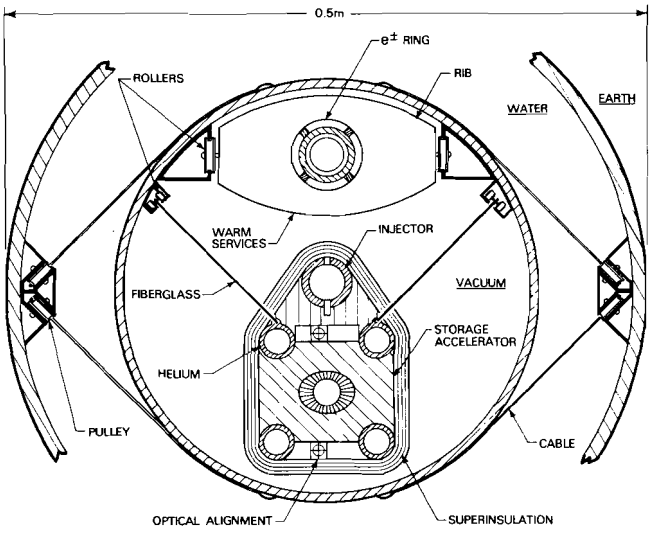

FIGURE 1. Cross section of tunnel. The cables supporting the neutral buoyancy cryostat at ~50m intervals are controlled from the ends of the long magnet sections.

TABLE II - Synchrotron Radiation. $N_p = 10^{15}$; $U_e = 0.05\ P_e$; $E_{ce} = 1.25$ MeV. Electron radiated power = 100 MW. N_p and N_e include two beams.

Proton-Antiproton						
P_s (TeV)	20		100		1000	
B_s (T)	2	5	2	5	2	5
R (km)	33.3	13.3	167	67	1670	667
I_p (ma)	229	573	46	115	4.6	11.5
U_p (MeV/turn)	0.037	0.094	4.7	11.7	4680	11700
T_p (days)	8.6	1.4	1.7	0.28	0.17	0.028
E_{cp} (keV)	0.086	0.215	2.15	5.4	215	540
Radiated Power (MW)	0.0086	0.054	0.214	1.34	21.4	134
Power gradient (W/m)	0.041	0.64	0.205	3.20	2.05	32.0
Beam Energy (GJ)	3.2	3.2	16	16	160	160
Electron-Positron						
P_e (TeV)	0.266	0.196	0.456	0.336	0.980	0.722
B_e (G)	266	490	91	168	20	36
N_e (10^{13})	3.3	1.8	9.5	5.2	44	24
I_e (ma)	7.5	10.2	4.4	5.9	2.0	2.8
T_e (sec)	0.028	0.011	0.14	0.156	1.4	0.56
Power gradient (W/m)	480	1200	96	240	9.6	24
Beam Energy (MJ)	1.4	0.56	6.9	2.8	69	28

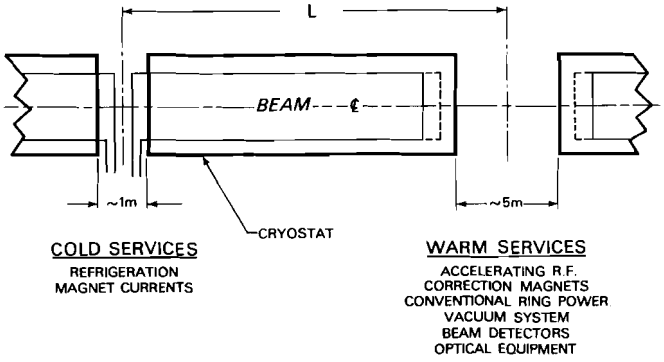

FIGURE 2. Schematic of normal ring segmentation. Magnets and related services are fed into the long cryostats from the warm service straight sections. Values of L are given in Table I.

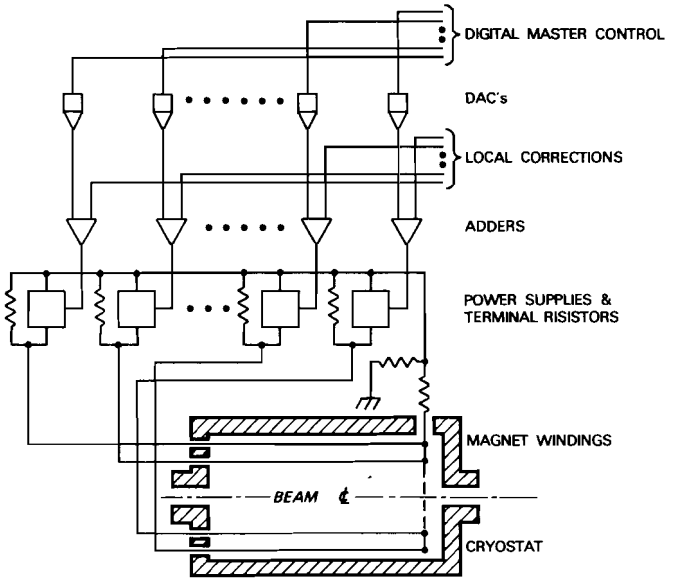

FIGURE 3. Schematic of magnet current source. Longitudinal superconductor elements of approximate length L are separately powered. Local corrections are for nonplanarity of orbit and other nonuniformities.

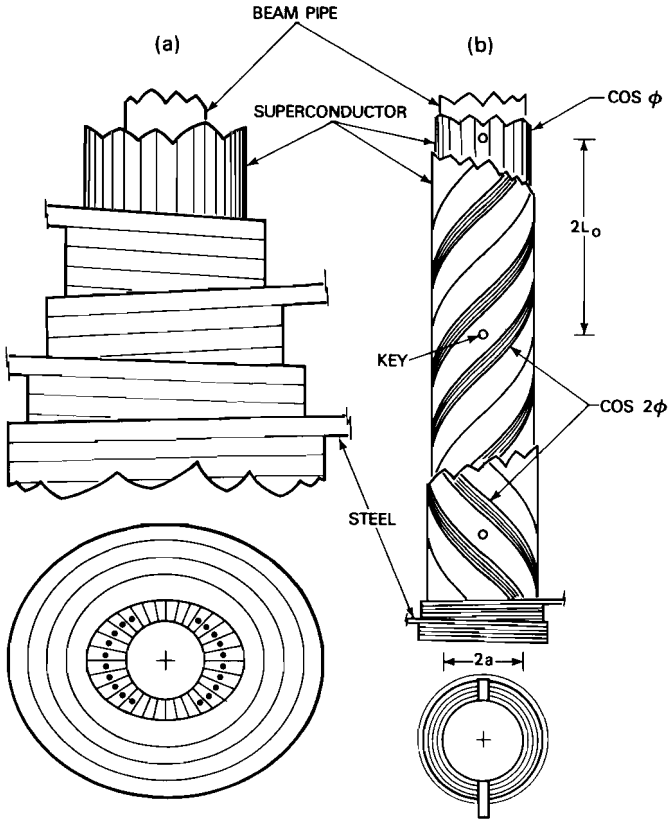

FIGURE 4. Superconducting magnet construction. The assembly lines are infinite and linear. a) 5T storage accelerator magnet showing wedge-shaped conductors compressed by a spiral-wrapped steel core. An alternative design is discussed in the text. b) Injector magnet. Thin windings, distributed as cosϕ (dipole) or cos 2ϕ (quadrupole), are superimposed. Quadrupole windings are each in two sets, spiral-wound with opposite helicities. The pitch is four times the effective magnet length, L_0 or L_1, given in Table I.